



OPEN Evaluation the toxic effects of Cobalt-Zinc Ferrite nanoparticles in experimental mice

Eman E. El-Nahass¹, B. I. Salem²✉, Sabry A. El-Naggar¹ & Mona M. Elwan¹

Cobalt Zinc ferrite nanoparticles (NPs) were synthesized utilizing the auto-combustion flash method, with the general formula $\text{Co}_{1-x}\text{Zn}_x\text{Fe}_2\text{O}_4$ ($x = 0, 0.35$). This study aimed to evaluate the hepato-renal and systemic toxicity of Cobalt Zinc Ferrite nanoparticles (CZF NPs). A total of eighty female mice were utilized to ascertain the median lethal dose (LD50) of CF NPs (100 mg/kg) and CZF NPs (100 mg/kg). Thirty female CD1 mice were placed into three groups, each containing ten animals. In Group 1 (Gp1), mice were administered a 200 μl injection of sterile saline intraperitoneally (i.p.). During a 6-day period, Gp2 and Gp3 received injections of CF NPs and CFZ NPs. On day 14 after injection, hematological, biochemical, and histopathological data were measured. CZF NPs were characterized using X-ray Diffraction Analysis (XRD), Transmission Electron Microscope (TEM) and Vibrating Sample Magnetometer (VSM). There was a significant alteration in the overall body weight of mice injected with CZF NPs. Injections of CF NPs did not significantly alter red blood cells (RBC) counts, hemoglobin concentration (Hb), hematocrit percentage (Hct%), total white blood cells (WBCs), and platelets. However, injections of CZF NPs resulted in an increase in WBC count and a decrease in platelet count. Furthermore, injection of CZF NPs altered the differential leukocyte percentages. The liver and kidney functions in mice injected with CF NPs did not show any notable changes. However, mice treated with CZF NPs had considerable increases in liver and kidney bio-markers. The administration of CF NPs did not modify the histological structure of hepatic and renal tissues; however, the hepatic and renal structures were disrupted in animals injected with CZF NPs. Overall, the findings indicated high toxicity of CZF NPs in the mice used for the experiment.

Keywords Toxicity, Cobalt-Zinc Ferrite, Nanoparticles, Mice, Histopathology, Liver, Kidney, XRD, Magnetization

Presently, nanoparticles (NPs) are utilized in many applications, particularly in the biomedical domain. NPs have shown promising results in treating various diseases. Nevertheless, it is important to note that NPs may exert harmful effects on certain essential organs¹. Nanomaterials, also known as NMs, are materials that are extremely small, often ranging in size from 1 to 100 nanometers. These materials have numerous benefits in delivering natural products for the treatment of cancer and other human ailments². Specifically, nanoparticles (NPs) were employed to enhance the transportation of nutrients into the cells³. The extraordinary properties of nanomaterials at reduced sizes are promising for an extensive number of industrial and medical applications⁴.

Nanotechnology is increasingly being used in various fields such as cytotoxicity, magnetic resonance imaging, biomedical applications, drug delivery, and cancer therapy^{5–10}. Spinel ferrite nanoparticles with various coatings have been extensively studied in the disciplines of biomedicine and bioengineering due to their favorable magnetic properties^{11–13}. These magnetic nanoparticles must possess magnetization values that are significantly high and a size that is less than 100 nanometers. Additionally, it is important for these materials to possess a low level of toxicity and a high degree of biocompatibility^{14,15}. The toxicity of nanoparticles on human health is a crucial factor for the successful implementation of nanoparticles in medicine.

Substituting divalent ions can alter magnetic, thermal, and electrical properties of spinel ferrites^{16–18}. The substitution of Co^{2+} with Zn^{2+} in CFO has an impact on the distribution of cations and brings about considerable changes in the magnetic and magnetoelastic characteristics¹⁹. Recent studies have demonstrated that Zn-doped CFO materials have great strain sensitivity, making them promising candidates for stress sensor applications. The amplitude of HC and magnetostriction decreases as the Zn^{2+} concentration increases, as revealed in studies

¹Zoology Department, Faculty of Science, Tanta University, Tanta 31527, Egypt. ²Physics Department, Faculty of Science, Tanta University, Tanta 31527, Egypt. ✉email: basant.salem@science.tanta.edu.eg

by^{20–23}. The Co^{2+} ions mostly contribute to the anisotropic features of CFO, whilst the Zn^{2+} ions are responsible for improving the dielectric and magnetic characteristics²⁴.

There are various synthesis methods for nano-ferrites include co-precipitation, microwave, electron-beam curing, sol-gel, citrate gel auto-combustion, high-energy ball milling, and thermal treatment^{25–28}. Among these methods, the sol-gel synthesis followed by thermal treatment is a quite simple and cost-effective approach. It involves using a minimal number of chemical components and has a shorter production time compared to other synthesis approaches²⁶.

In addition, nanoparticles (NPs) were employed as a precise method of delivering medicines, proteins, and genes²⁹. Biologically active nanoparticles (NPs) such as silver (Ag), gold (Au), titanium oxide, aluminum, cerium, zinc, and silicon have significant promises for many uses in biomedical and clinical research, particularly in cancer therapy and diagnostics³⁰. Nanoparticles (NPs) have been seen to trigger cell death, identify infections, immobilize enzymes, and are utilized in the application of magnetic fluid hyperthermia^{31,32}. Prior research has shown the utilization of Au and Ag nanoparticles in the therapy of cancer^{33,34}. For example, gold nanoparticles (Au NPs) have been employed in the treatment of skin cancer, whilst silver nanoparticles (Ag NPs) have been utilized in the treatment of breast and colon cancer^{35,36}. A previous study was done to synthesize the AgNPs and to investigate their impact on hormones, antioxidant enzymatic activities, and histopathology of the liver of albino mice³⁷.

There are two primary pathways via which nanoparticles (NPs) might enter the human body. Initially, nanoparticles (NPs) are breathed into the body by atmospheric air, namely through the upper respiratory tract. The act of breathing in metal nanoparticles such as iron (Fe), nickel (Ni), and titanium dioxide (TiO_2)³⁸. The second method, oral intake and entrance via the skin, either by injecting into the skin layer or absorbing through the skin pores, is mostly caused by exposure to medicinal or cosmetic products³⁹.

NPs have several practical applications, yet they nevertheless pose some risks to human health⁴⁰. For example, NPs have the potential to be detrimental to healthy tissues and cells, leading to significant repercussions⁴¹. Biodegraded NPs can build up inside cells and cause intracellular changes, such as the breakdown of organelle integrity or modifications in genes⁴². For example, Ag NPs had a very toxic effect on liver cells, resulting in a considerable reduction in mitochondrial activity. The microscopic analysis revealed that cells exposed to larger dosages of NPs exhibited aberrant changes in size, including cellular shrinkage and an irregular shape⁴³. Studies have indicated that inhaled NPs can enter the bloodstream and potentially affect many organs including the liver, heart, and lungs^{44,45}. The virus has the ability to spread from the lungs to other organs, including the brain, spleen, and perhaps the fetus in pregnant women^{46,47}. Serum activity levels of both AST and ALT were elevated, indicating hepatotoxicity caused by Ag NPs. In addition, Ag NPs were found to cause histological damage to the liver and kidney tissue^{48,49}. The presence of cadmium sulfide nanoparticles (CdS NPs) leads to an elevation in the concentration of creatinine in urine and significant harm to the proximal tubules, resulting in nephrotoxicity⁵⁰. Au NPs induce DNA damage and inflammation, resulting in fibrosis and pneumoconiosis, which leads to pulmonary toxicity⁴⁶. Previous research has demonstrated that silica nanoparticles can cause harm to the cardiovascular system, spinal cord, and nervous system, leading to oxidative stress, apoptosis, and toxicity^{51,52}.

Cobalt NPS (Co NPs) have a little inhibitory effect on the growth of ovarian cancer cells and do not harm normal cells. Furthermore, it has been found that the administration of Co NPs didn't cause any changes in the hematological parameters⁵³. The presence of Fe, Cu, Cr, V, and Zr NPS can lead to the generation of ROS, which in turn can cause DNA and cellular harm in the liver, kidney, muscle, brain, and pancreas⁵⁴.

Zinc oxide NPs (ZnO NPs) at high concentration caused notable alterations in liver enzymes, oxidative stress, liver, renal tissue, and the digestive system^{55,56}. The experiment also resulted in a notable reduction in serum glutathione levels and a considerable increase in serum MDA levels, leading to severe histopathological changes in the stomach and pancreatic cells, along with DNA breakage⁵⁷.

There are few reports on the toxicity of Fe_3O_4 , particularly in living organisms. Furthermore, several studies have obtained conflicting results. For example, several studies have indicated low levels of toxicity at certain dosages, while others have demonstrated non-toxic effects in living organisms^{58,59}. Previous studies have documented adverse effects on the liver, renal, gastrointestinal, and neurological systems in living organisms^{60,61}. Thus, this work was carried out to assess the hepatotoxic and nephrotoxic effects of Cobalt-Zinc Ferrite nanoparticles on liver and kidney tissues.

Materials and methods

Chemicals

Cobalt-Zinc ferrite nanoparticles (CZF NPs) were prepared in the Department of Physics, Faculty of Science, Tanta University. Serum alanine aminotransferase (ALT), serum aspartate aminotransferase (AST), creatinine and urea kits were purchased from Bio-diagnostic Company (Egypt).

CZFNPs preparation

Cobalt-Zinc ferrite nanoparticles were synthesized via the auto-combustion flash process, using the general formula $\text{Co}_{1-x}\text{Zn}_x\text{Fe}_2\text{O}_4$ (where $x = 0$ or 0.35). The flash approach employed Cobalt nitrate ($\text{Co}(\text{NO}_3)_2 \cdot 6\text{H}_2\text{O}$), Zinc nitrate ($\text{Zn}(\text{NO}_3)_2 \cdot 6\text{H}_2\text{O}$), Ferric nitrate ($\text{Fe}(\text{NO}_3)_3 \cdot 9\text{H}_2\text{O}$), and Urea ($\text{CO}(\text{NH}_2)_2$) as initial materials. Urea acts as a fuel for completing chemical reactions and causing internal ignition. The quantity of urea was determined utilizing the principle of charge neutrality. In a solution, the sum of all positive charges must equal the sum of all negative charges to maintain electrical neutrality. By considering the concentrations of all charged species present in the solution (e.g., ions, protons, hydroxide ions) and applying the charge balance equation, the concentration of urea can be determined, as described by⁶². The chemicals were accurately measured in the necessary stoichiometric ratios and were mixed in a beaker for 30 min while continuously stirring without

adding water. Metal nitrates possess hygroscopicity; consequently, they easily absorb moisture and become slurry. The mixture was then heated on a hot plate at 80 °C until it became viscous and internal ignition occurred, resulting in fine brown ferrite powder formation⁶³. The final as-prepared powder was ground for 30 min using a mortar. Preparation ensures accurate weighing and handling of chemicals to maintain stoichiometry and prevent contamination. The flow chart of the preparation method for the as-prepared fine powders is shown in Fig. (1).

Ethics Statement

This study was conducted in accordance with the ARRIVE guidelines for the ethical treatment, care, and use of animals in research. The experimental design, animal handling, and data collection procedures were carefully implemented to ensure reproducibility, transparency, and minimal animal suffering. Approval of the study was obtained from the international laboratory Animal Care and Use guidelines with ethical approval number (IAUCUC-SCI-TU-0232), and all procedures adhered to the appropriate ethical standards.

Experimental procedure

We analyzed our materials using X-ray diffraction (XRD) with a Philips model (PW-1729) diffractometer equipped with a Cu K α radiation source ($\lambda = 1.541178 \text{ \AA}$). The particles form and morphology were examined using a JEOL 1010 transmission electron microscope (TEM). The magnetization M was quantified in electromagnetic units per gram (emu/g) at standard room temperature. This measurement was conducted using a vibrating sample magnetometer (VSM) with the specific model number 1551 USA, manufactured by EG&G PARC.

Experimental animals

Female Swiss albino mice weighing $20 \pm 2 \text{ g}$ were purchased from the National Research Center (NRC) in Cairo, Egypt. The animals were kept in cages, with 6 animals per cage. Standard food and water were provided ad libitum, under a 12-h dark and 12-h light cycle at standard laboratory conditions of temperature and humidity. These conditions were maintained in a facility with controlled temperature and humidity. Prior to initiating the experiment, mice were housed for one week to allow for adaptation.

Determination of the medium lethal dose (LD₅₀)

Eighty female mice were used to determine the LD₅₀ of CZF NPs and CF NPs. In summary, various concentrations ranging from 1 to 5 g/kg of CZF NPs and CF NPs were produced and administered intraperitoneally (i.p.) to

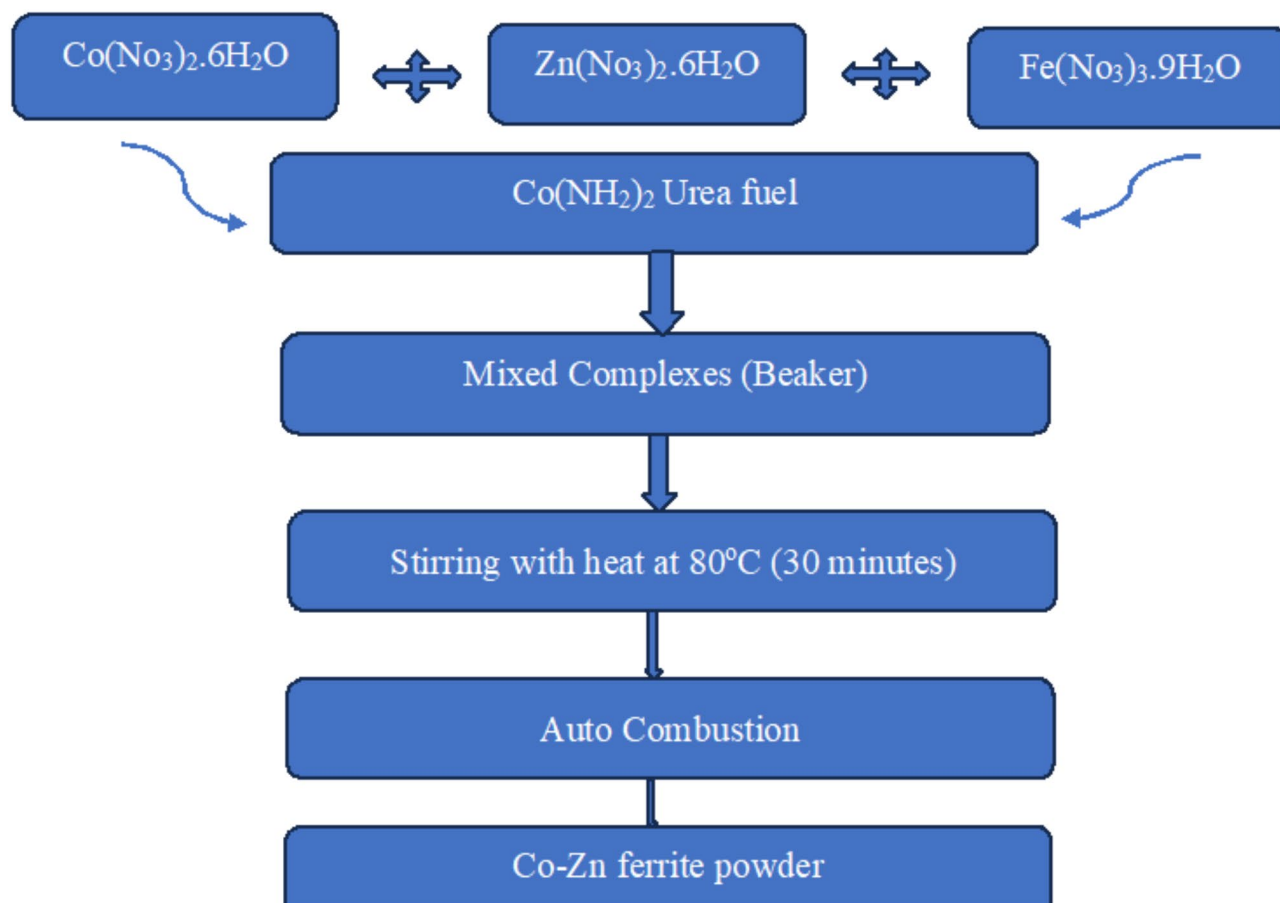


Fig. 1. Flow chart of the preparation method for cobalt zinc ferrite nanoparticles.

different groups. Injected mice were observed for 24 h to detect any toxicological characteristics to establish the LD₅₀. The LD₅₀ value was determined using Probit analysis, as described by Finney in 1971.

Experimental design

Thirty female CD-1 mice were allocated into three groups (10 mice /group) as follows: Group 1 (Gp1) was served as a negative control, injected with sterile saline (10 mL/kg) i. p. for 6 days. Gp2 was injected with CF NPs (100 mg/kg/ 6days) i.p. and Gp3 was injected with CZF NPs (100 mg/kg/ 6 days) i.p. Post 14 days, all groups were bled via the orbital plexus to collect blood for hematological and biochemical assessments. Mice were sacrificed on day 14 post-injection for sample collection. The method of euthanasia used in this study was inhalation of isoflurane, a commonly used anesthetic agent. Based on the molecular weight of isoflurane, we found that 20 ml is sufficient to anaesthetize an animal weighing 1000 g. Therefore, we can calculate the dose of anaesthetic for the animal using the following law: 20 ml of isoflurane X wt of mice/ 1000. For one mouse: Acquired dose = $20 \times 20 / 1000 = 0.4$ ml. So, 0.4 ml of isoflurane was sufficient to anaesthetize one mouse. Following anesthetization mice, they were subsequently euthanatized and dissected. The animals were exposed to a controlled concentration of isoflurane until loss of consciousness and respiration, followed by cervical dislocation to ensure human euthanasia in accordance with institutional guidelines and ARRIVE recommendations. Tissue samples were immediately collected for histological, hematological, and biochemical analyses.

Determination of body weight change

Mice from all experimental groups were weighed at the beginning (initial b.wt) and at the end of the experiments (final b.wt). The percentage of b.wt change % was calculated as follows: The percentage of b.wt change = $[(\text{final b.wt} - \text{initial b.wt}) / \text{initial b.wt}] \times 100$.

Hematological and biochemical analysis

The hematological parameters, including the total count of red blood cells (R.B.Cs), haemoglobin (Hb) concentration (g/dL), haematocrit (Hct) value (%), platelets count, as well as total and differential leucocyte counts, were determined using the auto hematology analyzer (BC-3200, Mindray, China). For biochemical analysis, blood samples were collected in heparinized glass tubes. The serum was separated from the blood samples using centrifugation at 3000 rpm for 15 min. The levels of ALT and AST were determined using commercially available kits⁶⁴. Commercial kits were used to test the amounts of serum creatinine and urea.

Histological investigations of liver and kidney tissues

Samples were taken from the liver and kidney from different experimental groups were fixed in 10% formal saline for 24 h. Then were dehydrated in ascending series of alcohol, cleared in xylene, and embedded in paraffin wax at 56 °C for 24 h. Paraffin sections of 4-μm thickness were collected on glass slides, dewaxed in xylene, hydrated in descending series of alcohol, stained by hematoxylin and eosin stains, dehydrated in ascending series of ethyl alcohol, cleared in two changes of xylene, and mounted with DPX. Finally, slides were examined by light electric microscope (Olympus, CX41, Japan)⁶⁵.

Statistical analysis

Data were presented as mean ± SD and were analyzed using one-way analysis of variance (ANOVA) followed by Dunnet test and $p < 0.05$ or $p < 0.01$ were statistically significant.

Results

X-ray diffraction analysis (XRD)

Figure 2 shows the XRD pattern of Co_{1-x}Zn_xFe₂O₄ nanoparticles, where x denotes the variable content of zinc (Zn) in the nanoparticles, with values ranging from 0 to 0.35. The X-ray diffraction (XRD) patterns of cobalt zinc ferrite nanoparticles resemble the diffraction patterns of the pure cubic spinel phase CoFe₂O₄ (JCPDS card no. 22-1086)⁶⁶. The observed peaks at ($2\theta = 17.5^\circ, 30.28^\circ, 35^\circ, 37^\circ, 42.7^\circ, 53.2^\circ, 56.2^\circ, 62.6^\circ, 71.2^\circ$ and 75.2°) can be attributed to scattering from the (111), (220), (311), (222), (400), (422), (511), (440), (533) and (622) planes correspondingly.

Adding Zn ($x = 0.35$) to the samples results in an increase in the intensity of diffraction peaks and the resolution (step size) was 0.05 degree/minute which is sufficient to detect all phases. In addition, the doped samples exhibit a shift towards higher angles in the unique peaks (311), (220), and (440) compared to CoFe₂O₄, with the peak position being $x = 0.35$. The increase in the maximum level of intensity is influenced by the quantity of Zn present^{67,23}. Scherer's formula,

$$D = 0.9 \lambda / \beta \cos \theta \quad (1)$$

is utilized to compute the size of crystallite. The symbol D represents the size of the crystallite, λ represents the wavelength of X-ray radiation (0.154 nm), β represents the complete width of the diffraction line at half the maximum intensity measured in radians, and θ represents the Bragg angle. Table 1 presents the values for the crystallite size, x-ray density, bulk density, porosity, and particle size of the two compositions.

High Resolution Transmission Electron Microscopy Analysis (HRTEM)

The HRTEM analysis was conducted to examine the shape and microstructure of Co_{1-x}Zn_xFe₂O₄ ($x = 0, 0.35$) nanoparticles, as seen in Fig. 3. The micrographs reveal that the particles exhibit uniformity in size and possess

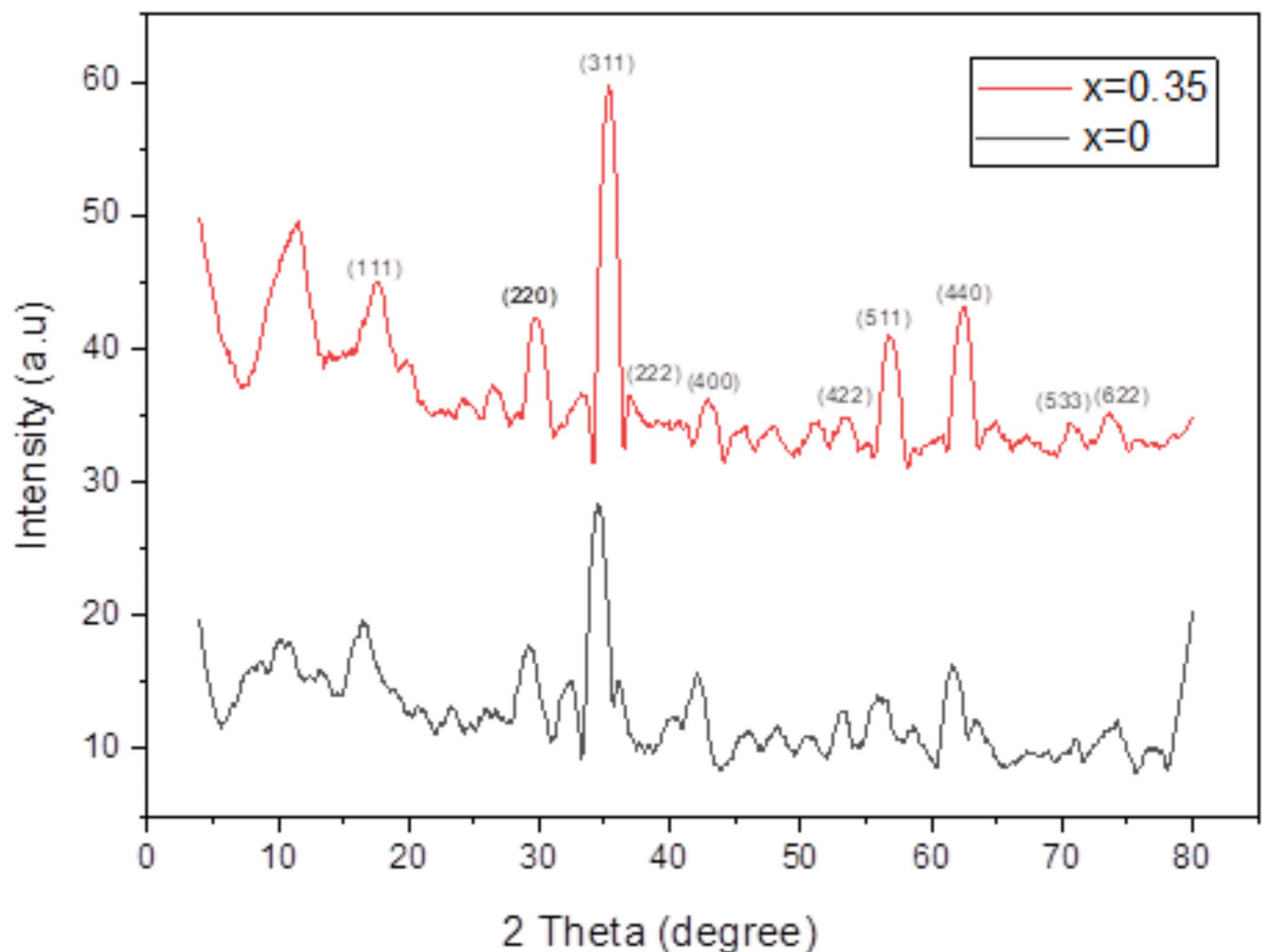


Fig. 2. XRD of $\text{Co}_{1-x}\text{Zn}_x\text{Fe}_2\text{O}_4$ ($x=0,0.35$) nanoparticles.

x	a_{exp} (Å)	D_x (g/cm ³)	D (g/cm ³)	P (%)	t_{XRD} (nm)	t_{TEM} (nm)
0.0	8.37	4.59	2.49	54.40	19.30	17.85
0.35	8.38	4.88	2.59	53.80	26.95	28.51

Table 1. Experimental lattice parameter (a_{exp}), X-ray density (D_x), bulk density (D), porosity (P) Average crystallite size (t_{XRD}) and particle size (t_{TEM}) of $\text{Co}_{1-x}\text{Zn}_x\text{Fe}_2\text{O}_4$ ($x=0,0.35$) nanoparticles.

an approximately spherical shape. Table 1 shows that the estimated average particle size of CoFe_2O_4 and $\text{Co}_{0.65}\text{Zn}_{0.35}\text{Fe}_2\text{O}_4$ nanoparticles.

The mean particle size of nanoparticles with $x=0$ was lower than that of nanoparticles with $x=0.35$, which can be attributed to the lesser ionic radius of Co^{2+} ions (0.83 Å) compared to Zn^{2+} ions (0.88 Å). Figure 3 displays the selected area electron diffraction (SAED) pattern of CoFe_2O_4 and $\text{Co}_{0.65}\text{Zn}_{0.35}\text{Fe}_2\text{O}_4$ nanoparticles. The pattern exhibits a ring-like arrangement of spots, which suggests the highly crystalline nature of the samples and has good agreement with XRD pattern.

Vibrating Sample Magnetometer Analysis (VSM)

Figure 3 displays the magnetic hysteresis loops of $\text{Co}_{1-x}\text{Zn}_x\text{Fe}_2\text{O}_4$ ($x=0,0.35$) nanoparticles. These measurements were conducted at ambient temperature and covered a magnetic field range of roughly -20 to $+20$ kOe. Figure 4 demonstrated that increasing the Zn-doping in CoFe_2O_4 nanoparticles will alter the magnetic properties of the samples.

Table (2) displays the range of values for saturation magnetization (M_s), remanent magnetization (M_r), and coercivity field (H_c) for all specimens. The coercivity value exhibited a decrease as the Zn concentration (x) increased. The magnetic saturation values of M_s and M_r exhibited an upward trend with the progressive

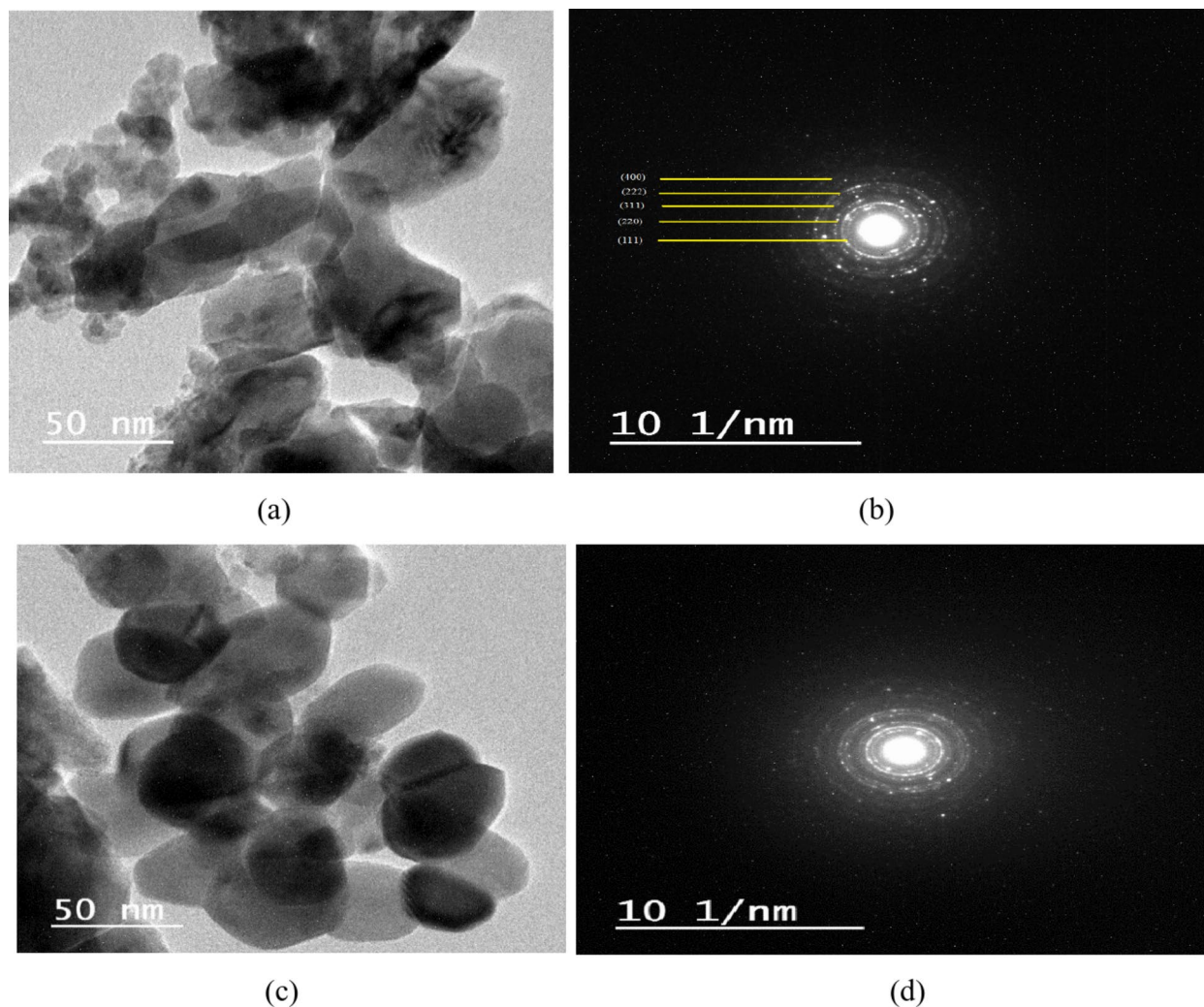


Fig. 3. HRTEM microstructures of (a) CoFe₂O₄, (c) Co_{0.65}Zn_{0.35}Fe₂O₄ and SAED pattern of (b) CoFe₂O₄, (d) Co_{0.65}Zn_{0.35}Fe₂O₄ nanoparticles.

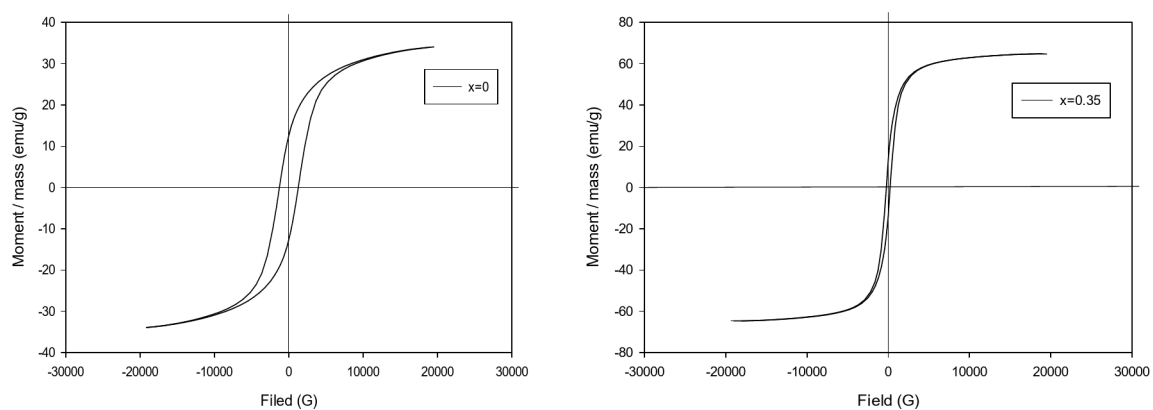


Fig. 4. Hysteresis loops of (a) CoFe₂O₄, (b) Co_{0.65}Zn_{0.35}Fe₂O₄ nanoparticles.

x	H _c (Oe)	M _s (emu/g)	M _r (emu/g)	M _r /M _s
0	1277.8	34.052	12.585	0.369
0.35	237.51	64.795	13.176	0.203

Table 2. Coercivity (H_c), saturation magnetization (M_s), Remanent magnetization (M_r) for Co_{1-x}Zn_xFe₂O₄ (x=0,0.35) nanoparticles.

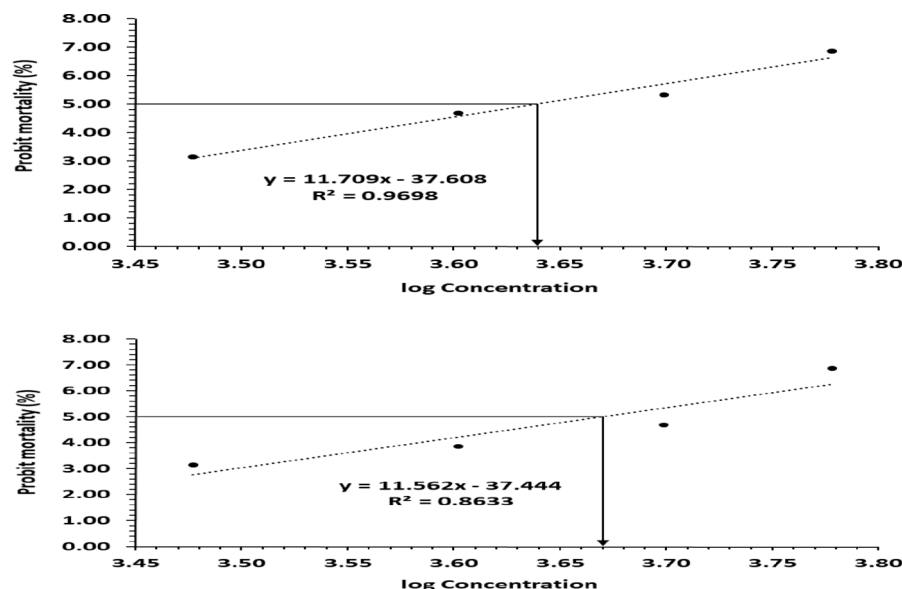


Fig. 5. (A, B) : Determination of LD₅₀ of CF NPs and CZF NPs on albino Swiss mice.

incorporation of Zn into CoFe₂O₄ nanoparticles, rising from 34.05 to 64.79 emu/g and 12.58 to 13.17 emu/g, respectively, as indicated in Table 2.

CF NPs and CZF NPs LD₅₀ post 24 h. of I.P. injection

Different dosages of CF NPs and CZF NPs were generated and given to ascertain the median lethal dose (LD₅₀) post 24 h. of injection. The concentrations varied from 1 to 5 g/kg. The findings demonstrated that the LD₅₀ of CF NPs and CZF NPs were 4.3 and 4.6 g/kg, respectively (Fig. 5A, B).

CZF NPs injection decreased the percentage of body weight changes

Groups of mice that injected with CF NPs (1/40 LD₅₀) and CZF NPs (1/40 LD₅₀) for 6 days were noticed for body weight changes (b.wt%). The findings indicated that CF NPs injected mice were similar in regard to % of b.wt changes to the control group. While there was a notable difference in the overall body weight in CZF NPs injected mice when compared to their control (Fig. 6). The % b.wt change in the group of mice which were injected with CF NPs and CZF NPs were 53.4 and 11.1 respectively.

Injection of CZF NPs 6 days altered some hematological parameters

The data shown in Table 3 indicates that the administration of CF NPs did not cause any significant changes in the levels of total red blood cells (RBCs), hemoglobin concentration (Hb), hematocrit percentage (Hct%), total white blood cells (WBCs), and platelets, as compared to the control values. Nevertheless, the administration of CZF NPs injection daily for 6 days resulted in an elevation in WBCs count and a reduction in the platelets count. The findings indicated that the administration of CF NPs did not modify the differential leukocyte percentages. Nevertheless, the introduction of CZF NPs caused changes in these percentages. In the group of mice injected with CZF NPs, the percentages of lymphocytes, neutrophils, and monocytes were 51.3%, 29.7%, and 16.7% respectively (Table 4).

CZF NPs injection led to hepatorenal dysfunction

The findings indicated that administering CF NPs to the mice group for 6 days did not induce any changes in the liver transaminases enzymes (ALT and AST) and did not result in any alterations in the levels of urea and creatinine, as compared to the control group. In addition, this study revealed that the injection of CZF NPs in mice led to a rise in ALT and AST activities, as well as elevated levels of urea and creatinine (Table 5).

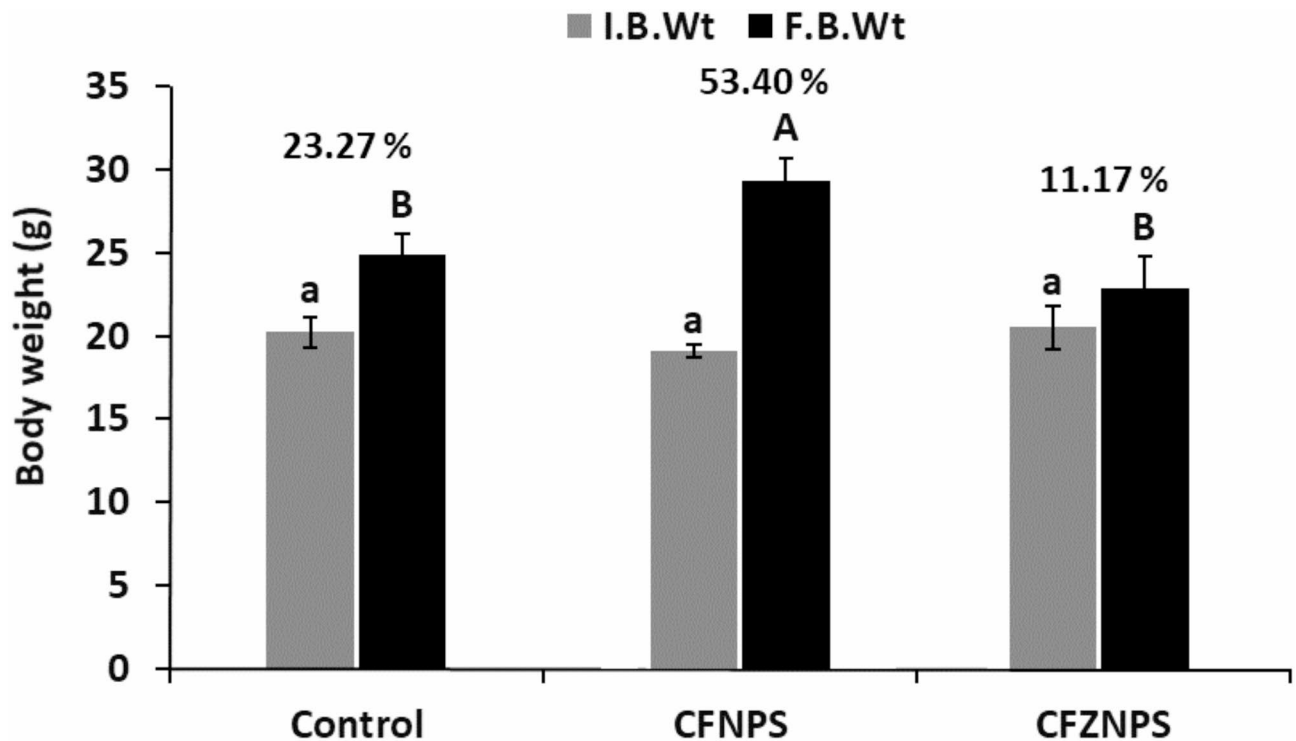


Fig. 6. Initial and final weight of different groups under the study.

Groups	R.B.Cs ($\times 10^6/\mu\text{L}$)	Hb (g/dL)	Hct (%)	W.B.Cs ($\times 10^3/\mu\text{L}$)	Platelets ($\times 10^3/\mu\text{L}$)
Control	6.67 ± 1.7^a	12.97 ± 0.9^a	39.2 ± 2.5^a	7.43 ± 1.4^b	968.88 ± 76.7^a
CF NPs	7.9 ± 0.6^a	12.4 ± 0.8^a	37.6 ± 1^a	8.8 ± 2.9^b	881.7 ± 198.6^a
CFZ NPs	8.5 ± 0.5^a	13.1 ± 1.6^a	38.2 ± 4.9^a	16.3 ± 3.9^a	795 ± 113^b

Table 3. The hematological parameters of mice treated with CF NPs or CFZ NPs for 6 days. The values represented mean \pm SD. CF NPs: Cobalt Ferrite Nanoparticles, CFZ NPs: Cobalt Ferrite Zinc Nanoparticles.

Groups	Total number of different leukocytes ($\times 10^3/\mu\text{L}$)		
	Monocytes ($\times 10^3/\mu\text{L}$)	Lymphocytes ($\times 10^3/\mu\text{L}$)	Neutrophils ($\times 10^3/\mu\text{L}$)
Control	2.67 ± 0.58^b	80.33 ± 6.51^a	17.0 ± 5^a
CF NPs	13.3 ± 9.5^a	71 ± 13^a	15.7 ± 3.5^c
CFZ NPs	16.7 ± 4.8^a	51.3 ± 36.5^b	29.7 ± 47.1^b

Table 4. Absolute numbers of the differential leucocytes in different groups under the study. The values represented mean \pm SD. CF NPs: Cobalt Ferrite Nanoparticles, CFZ NPs: Cobalt Ferrite Zinc Nanoparticles.

Groups	AST (U/l)	ALT (U/l)	Urea (mg/dl)	Creatinine (mg/dl)
Control	173 ± 8.9^b	48 ± 3.5^a	35 ± 3.2^a	0.38 ± 0.05^a
CF NPs	180 ± 13.9^a	47 ± 3.6^a	35.7 ± 14.6^a	0.4 ± 0.06^a
CFZ NPs	217 ± 19.7^b	59.7 ± 9.9^b	48 ± 11.1^b	0.47 ± 0.05^b

Table 5. AST, ALT, urea and creatinine levels in different groups of mice treated with CF NPs or CFZ NPs. The values represented mean \pm SD. CF NPs: Cobalt Ferrite Nanoparticles, CFZ NPs: Cobalt Ferrite Zinc Nanoparticle.

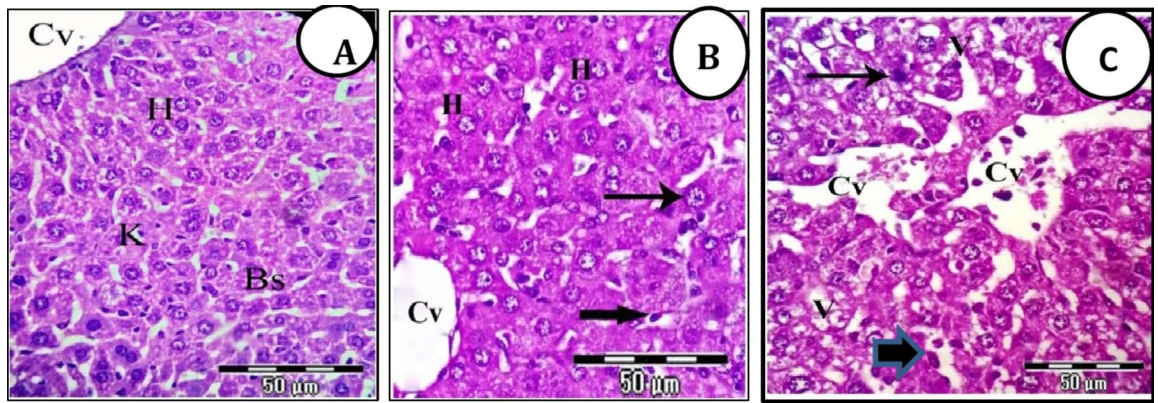


Fig. 7. (A–C). Photomicrographs of liver sections stained with H&E showing. (A) Liver sections of control mice exhibit normal hepatic architecture, normal central vein (Cv), normal hepatic strands (H), and regular blood sinusoids (Bs) lined with normal phagocytic Kupffer cells (K). (B) Liver sections of mice of CF NPs group showing normal like structure of hepatic construction, normal central vein (Cv), irregular hepatic strands (H) with normal nuclei have regular distribution of chromatin, other hepatocytes with megakaryocytic nuclei (arrows), and irregular blood sinusoids with distinct phagocytic Kupffer cells (thick arrow). (C) Liver sections of mice of CZF NPs group exhibit disorganization of hepatic manner, irregular and congested central veins (Cvs), some hepatocytes with pyknotic nuclei (arrows), others with vacuolated cytoplasm (V) and widening blood sinusoids with distinct phagocytic Kupffer cells (thick arrow) were noticed (X 400).

CZF NPs induced hepatic-architecture alterations

Microscopic examination of liver sections of control group (Gp1) showed normal strands of hepatocytes had homogenous granular cytoplasm with centrally located nucleus. The liver strands were alternating with homogenous granular cytoplasm with centrally located nucleus. The liver strands were alternating with blood sinusoids lined by endothelial cells and distinct phagocytic Kupffer cells (Fig. 7A). Treatment of the mice with narrow CF NPs exhibited normal like structure of hepatic construction, normal central vein, irregular hepatic strands, hepatocytes with normal nuclei, other hepatocytes with megakaryocytic nuclei, and irregular blood sinusoids with distinct phagocytic Kupffer cells were also seen (Fig. 7B). While treatment of the mice with CZF NPs showed disorganization of the hepatic manner, irregular and congested central veins, some hepatocytes with pyknotic nuclei, others with vacuolated cytoplasm and widening blood sinusoids with distinct phagocytic Kupffer cells were noticed (Fig. 7C).

CZF NPs induced renal architecture alterations

Microscopic examination of kidney sections of control group (Gp1) showed normal renal cortex, normal glomeruli and normal renal tubules (Fig. 8A). Kidney section of mice of CF NPs group exhibited normal glomeruli with regular Bowman's space, few numbers of renal tubules are distended and dilated, others are damaged, and their lining epithelial cells became undistinguished, and their contents were intermixed with each other (Fig. 8B). While Kidney section of mice of CZF NPs group revealed disorganized glomeruli with irregular Bowman's space, mostly renal tubules were damaged and lost their characteristic appearance, others were occluded with hyaline casts and their nuclei are darkly stained (Pyknotic nuclei) (Fig. 8C).

Discussion

Recent studies indicate that spinel ferrite nanoparticles may have harmful effects on human cells, despite their many benefits^{68–70}. While cobalt ferrite (CoFe_2O_4) has received significant attention for its positive effects in medicinal applications, it is crucial to evaluate its possible risks to both humans and the environment. Nanoparticles (NPs) may have harmful consequences due to their small size and unique physicochemical features⁷¹. Therefore, it is essential to comprehensively describe the nanoparticles prior to conducting their toxicological examinations. The size, shape, crystallinity, and agglomeration/dispersion of NPs are important factors that influence their biological interactions^{72,71,73}. We utilized XRD, TEM, and VSM methods to analyze and describe the NPs.

The XRD pattern reveals that the diffraction peaks have a cubic structure, and the degree of sharpness of these peaks shows the level of crystallinity of the samples, with absence of secondary phases or contaminants. The lattice constant (a_{exp}) for CZF NPs was greater than that of CF NPs. The probable cause of this phenomenon is the dispersion of zinc ions into the tetrahedral sites, resulting in an expansion of the lattice parameter of CZF NPs. This finding is supported by another study⁷⁴. The TEM micrographs show that the particles have a uniform size and are approximately spherical in shape which agree with⁷⁴. The average particle size is 17.85 nm for CF NPs and 28.5 nm for CZF NPs. This confirms the creation of nanoparticles, and the results are consistent with those obtained from X-ray diffraction. The results of the VSM analysis indicated that higher levels of Zn-doping in the CoFe_2O_4 nanoparticles would result in a transition of the magnetic properties of the samples from low magnetic properties to high ones. The observed increase in saturation magnetization (M_s) with Zn doping is consistent with findings reported by⁷⁴. Compared to²³, our Zn-doped samples exhibited a notably higher saturation magnetization (64.79 emu/g at $x=0.35$), which may reflect differences in synthesis methods,

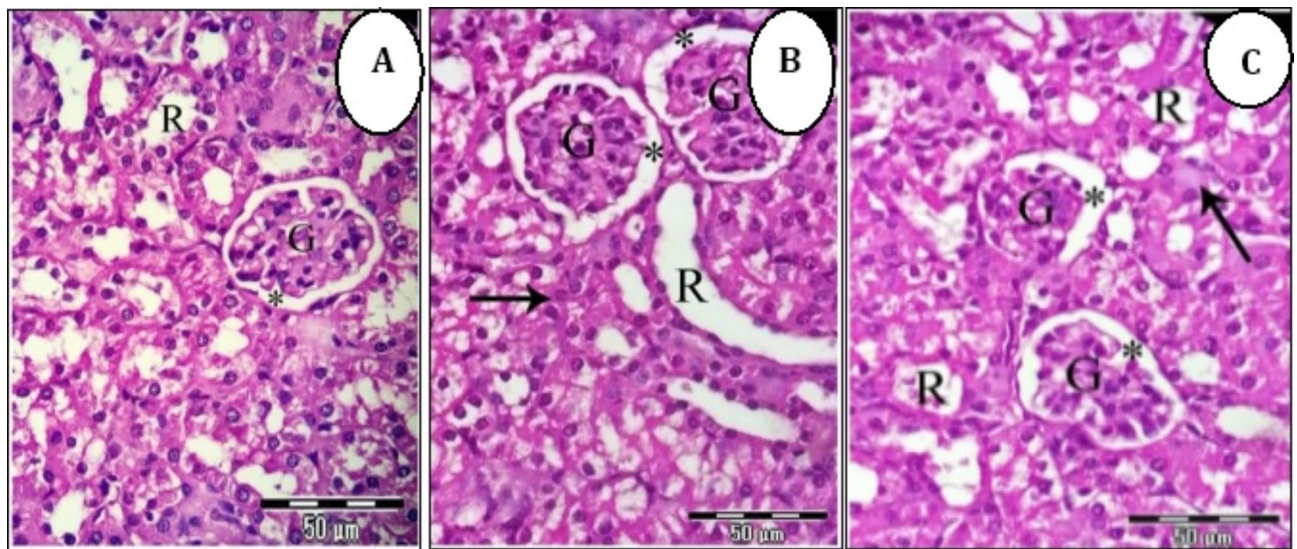


Fig. 8. (A–C). Photomicrographs of kidney sections stained with H&E showing. (A) Kidney section of control mice showed normal renal cortex, normal glomeruli (G) and normal renal tubules (R). (B) Kidney section of mice of CF NPs group exhibited normal glomeruli (G) with regular Bowman's space (*), few number of renal tubules are distended and dilated (R), others are damaged and destroyed (arrow), and their lining epithelial cells became undistinguished, and their contents were intermixed with each other. (C) Kidney section of mice of CZF NP group showed that disorganized glomeruli (G) with irregular Bowman's space (*), mostly renal tubules were damaged and lost their characteristic appearance (R), others were occluded with hyaline casts (arrows) (X 400).

particle size, or Zn distribution. This suggests that our synthesis approach may yield materials with superior magnetic properties for certain applications. The auto-combustion flash process used in this study appears to yield particles with improved crystallinity and magnetic properties compared to co-precipitation method reported in⁷⁵. The low coercive force indicates that the cobalt-zinc ferrite ($x=0.35$) possesses characteristics of a soft ferrite and slim hysteresis loop, where the sample CoFe_2O_4 ($x=0$) has the threshold characteristic of hard ferrite and the presence of considerable area of hysteresis loop. It behaves as a semi hard ferrite. Similarly, the reduction in coercivity (H_c) with increasing Zn content has been widely documented⁷⁶. The Zn ions help the magnetic moment of the ions in $\text{CoZnFe}_2\text{O}_4$ to reoriented to their original position in fast and easy process with the decreasing of the external magnetic field.

Toxicity is a critical factor which should be considered during evaluating potential biomedical use of NPs in vivo applications. The objective of this study was to assess the hepatotoxic and nephrotoxic effects of CF NPs and CZF NPs on liver and kidney tissues. The current investigation identified the median fatal concentration of CF NPs and CZF NPs, which caused the death of 50% of mice. The reported values were 4.3 and 4.6 g/kg, respectively. In their investigation⁷⁷, found that the cobalt ferrite nano-complex had an LD50 of (25×10^{-9} M and 50×10^{-9} M) after 25 and 72 h, respectively, indicating acute toxicity. The results indicated that mice injected with CF NPs had similar changes in body weight% compared to the normal control group. There was a notable difference in the overall body weight of mice injected with CZF NPs compared to the control group. The decrease in body weight% following CZF NPs injection suggests that this compound may have a harmful impact on the organs of the body. This conclusion aligns with recent research conducted by^{78,56}, which showed a decrease in body weight alterations following the injection of mice with ZNO NPs.

The mice that were injected with CF NPs didn't exhibit any changes in the levels of RBCs, Hb, Hct, % W.B. Cs, and platelets compared to their control values. These findings contrasted with⁵³, who demonstrated that less than 5% hemolysis indicated the compatibility of Co NPs with human RBCs. However, the administration of CZF NPs by injection leads to a notable rise in the total number of white blood cells (W.B. Cs) and the percentages of lymphocytes, neutrophils, and monocytes. Conversely, there is a drop in the count of platelets. The findings of our study showed that the injection of CF NPs didn't cause any changes in the percentages of different types of leukocytes. Nevertheless, the introduction of CZF NPs caused an alteration in these proportions. The results also indicated that the injection of CF NPs didn't alter the levels of AST and ALT in the serum. However, there was a considerable rise in CZF NPs injected mice compared to their control group. The substitution of Zn in the ferrite structure can indeed increase the toxicity of CZF NPs compared to CF NPs. Zn substitution can potentially increase the bioavailability and toxicity of the nanoparticles. It may affect the biodistribution and accumulation of the nanoparticles in tissues, potentially leading to higher concentrations in sensitive organs and increased toxicity. The results of this study were consistent with prior research, which showed that high concentrations of ZnO NPs caused the accumulation of these particles in the liver. This accumulation led to harmful effects on liver tissue, including cellular alterations and a large rise in liver enzymes⁵⁵. In the present investigation, administration of CF NPs did not result in any notable alteration in the levels of urea and creatinine, as compared

to the control group of mice. However, these levels were considerably elevated in the mice treated with CZF NPs. These parameters are commonly considered to be dependable indicators of renal injury⁷⁹. Furthermore, serum creatinine has been utilized as a means to assess glomerular function, with its elevation serving as a signal of renal failure⁸⁰.

This study established a correlation between hematological, biochemical, and histological markers. The histopathological changes observed in the group of mice injected with CZF NPs included significant disruption of liver structure, with degeneration and death of numerous hepatocytes, cytoplasmic vacuolation, noticeable nuclear alterations such as pyknotic nuclei, increased blood vessel congestion, and aggregation of inflammatory cells. Similar results were recorded by⁸¹. The liver sections of mice injected with CF NPs exhibited a hepatic architecture that was mostly normal, with some minor alterations seen such as blood vessel congestion and expansion of blood sinusoids. Furthermore, our findings indicated that mice treated with CF NPs had a healthy renal cortex, intact glomeruli with regular Bowman's space, and normal renal tubules. The mice injected with CZF NPs exhibited histological changes in their kidney tissues, including damaged and shrunken glomeruli with irregular Bowman's space, as well as loss of characteristic appearance of the renal tubules. Additionally, intertubular hemorrhage was observed. These findings align with a study by⁸², which demonstrated that ZnO NPs induce histopathological alterations in the kidney through oxidative stress.

Conclusion

This research investigates the impact of Zn^{2+} ion doping on the structural, morphological, and magnetic characteristics of $\text{Co}_{1-x}\text{Zn}_x\text{Fe}_2\text{O}_4$ ($x = 0, 0.35$) nanoparticles. Replacing Zn^{2+} ions lead to an expansion of the lattice parameter. The reduction in coercivity from 1277.8 to 237.51 Oe, achieved by increasing the zinc concentration, can be ascribed to the magnetic properties and anisotropic nature of cobalt.

The data obtained suggest that CZF NPs exhibited toxicity towards liver and kidney tissues, as seen by elevated levels of AST, ALT, urea, and creatinine at concentrations of 1/40 4.6 g/kg, leading to hepato-renal dysfunction. In contrast, CF NPs were found to be non-toxic at concentrations of 1/40 4.3 g/kg.

Data availability

All data generated or analyzed during this study are included in this published article. More detailed data is available from the corresponding author on reasonable request.

Received: 15 November 2024; Accepted: 10 February 2025

Published online: 26 February 2025

References

- Xuan, L., Ju, Z., Skonieczna, M., Zhou, P. K. & Huang, R. Nanoparticles-induced potential toxicity on human health: Applications, toxicity mechanisms, and evaluation models, *MedComm*. 4: e327 (2023). <https://doi.org/10.1002/mco2.327>
- Patra, J. K. et al. Shin. HS. Nano based drug delivery systems: recent developments and future prospects. *J. Nanobiotechnol.* Volume. 16 (71), 16–71. <https://doi.org/10.1186/s12951-018-0392-8> (2018).
- Acosta, P. Bioavailability of nanoparticles in nutrient and nutraceutical delivery. *J. Int. Econ.* 79 (1), 102–116. <https://doi.org/10.1016/j.cocis.2008.01.002> (2009).
- Umar, A., Khan, M. S., Wajid, M. & Khan, M. *U BioNanoScience* 14:3078–3098, <https://doi.org/10.1007/s12668-024-01598-4>. (2024).
- Debouttière, P. J., Roux, S., Vocanson, F., Billotey, C. & Beuf, O. Design of gold nanoparticles for magnetic resonance imaging. *Adv. Funct. Mater.* 16, 2330–2339 (2006).
- Gryparis, E. C., Hatzia Apostolou, M., Papadimitriou, E. & Avgoustakis, K. Anticancer activity of cisplatin-loaded PLGA-mPEG nanoparticles on LNCaP prostate cancer cells. *Eur. J. Pharm. Biopharm.* 67, 1–8 (2007).
- Jain, T. K., Richey, J., Strand, M., Leslie-Pelecky, D. L. & Flask, C. A. Magnetic nanoparticles with dual functional properties: drug delivery and magnetic resonance imaging. *Biomaterials* 29, 4012–4021 (2008).
- Horák, D., Babic, M., Jendelová, P., Herynek, V. & Trchová, M. *J. Magn. Magn. Mater.* 321: 1539 (2009).
- Yallapu, M. M., Othman, S. F., Curtis, E. T. & Gupta, B. K. Jaggi, M. Multifunctional magnetic nanoparticles for magnetic resonance imaging and cancer therapy. *Biomaterials* 32, 1890–1905 (2011).
- Ge, G., Wu, H., Xiong, F., Zhang, Y. & Guo, Z. The cytotoxicity evaluation of magnetic iron oxide nanoparticles on human aortic endothelial cells. *Nanoscale Res. Lett.* 8, 1–10 (2013).
- Girgis, E., Wahsh, M. M., Othman, A. G., Bandhu, L. & Rao, K. Synthesis, magnetic and optical properties of core/shell $\text{Co}_{1-x}\text{Zn}_x\text{Fe}_2\text{O}_4/\text{SiO}_2$ nanoparticles. *Nanoscale Res. Lett.* 6, 460 (2011).
- Doulabi, F. M. & Mohsen-Nia, M. Magnetic cobalt-zinc ferrite/PVAc nanocomposite: synthesis and characterization. *Iran. Polym. J.* 22, 9–14 (2013).
- Hoque, S. M., Srivastava, C., Srivastava, N., Venkateshan, N. & Chattopadhyay, K. *J. Mater. Sci.* 48: 812 (2013).
- Cullity, B. D. & Stock, S. R. Elements of X-ray Diffraction; Prentice Hall Upper Saddle River, NJ (2001).
- Muroi, M., Street, R., McCormick, P. & Amighian J. *Phys. Rev. B* 63:184414 (2001).
- Ashour, A. H. et al. Antimicrobial activity of metal-substituted cobalt ferrite nanoparticles synthesized by sol-gel technique. *Particuology* 40, 141–151 (2018).
- Anu, K. & Hemalatha, J. Magnetic and electrical conductivity studies of zinc doped cobalt ferrite nanofluids. *J. Mol. Liq.* 284, 445–453 (2019).
- Dippong, T., Goga, F., Levei, E. A. & Cadar, O. Influence of zinc substitution with cobalt on thermal behavior, structure and morphology of zinc ferrite embedded in silica matrix. *J. Solid State Chem.* 275, 159–166 (2019).
- Bhame, S. D. & Joy, P. A. Enhanced strain sensitivity in magnetostrictive spinel ferrite $\text{Co}_{1-x}\text{Zn}_x\text{Fe}_2\text{O}_4$. *J. Magn. Magn. Mater.* 447, 150–154 (2018).
- Tatarchuk, T. R. et al. Effect of cobalt substitution on structural, elastic, magnetic and optical properties of zinc ferrite nanoparticles. *J. Alloys Comp.* 731, 1256–1266 (2018).
- Dippong, T. et al. Thermal behavior of Ni, Co and Fe succinates embedded in silica matrix. *J. Therm. Anal. Calorim.* 136, 1587–1596 (2019).
- Naik, M. M. et al. Green synthesis of zinc doped cobalt ferrite nanoparticles: structural, optical, photocatalytic and antibacterial studies. *Nano-Struct Nano-Objects.* 19, 100322 (2019).

23. Zamani, M. et al. $\text{Co}_{1-x}\text{Zn}_x\text{Fe}_2\text{O}_4$ based nanocarriers for dual-targeted anticancer drug delivery: synthesis, characterization, and in vivo and in vitro biocompatibility study. *J. Mol. Liq.* **274**, 60–67 (2019).
24. Atif, M. et al. Synthesis and investigation of structural, magnetic and dielectric properties of zinc substituted cobalt ferrite. *J. Pys Chem. Solids*. **123**, 36–42 (2018).
25. Nayeem, F., Parveez, A., Chaudhuri, A., Sinha, R. & Khader, S. A. Effect of Zn^{+2} doping on structural, dielectric and electrical properties of cobalt ferrite prepared by auto combustion method. *Mater. Today Proc.*, 4, 12138–12143 (2017).
26. Chakradhar, V. K., Ansari, A. & Jaleel, A. M. Design, synthesis, and testing of high coercivity cobalt doped nickel ferrite nanoparticles for magnetic applications. *J. Magn. Magn. Mater.* **469**, 674–680 (2019).
27. El Foulani, A. H. et al. Effect of surfactants on the optical and magnetic properties of cobalt-zinc ferrite $\text{Co}_{0.5}\text{Zn}_{0.5}\text{Fe}_2\text{O}_4$. *J. Alloys Comp.* **774**, 1250–1259 (2019).
28. Khan, M. U. et al. Metal Nanoparticles: Synthesis Approach, Types and Applications – A Mini Review (2023).
29. Zhang, F., Kitamoto, Y., Abe, M. & Naoe, M. Effect of Ni addition into Co ferrite thin films for perpendicular recording media. *J. Appl. Phys.* **87**, 6881–6883 (2000).
30. Hendrikson, O. D., Safenkova, I., Anatoly, V., Vladimir, Z. & Popov, O. Methods of detection and identification of manufactured nanoparticles. *Biofizika* **56** (6), 965–994 (2011).
31. Wang, M. D., Shin, D. M., Simons, J. W. & Nie Nanotechnology for targeted cancer therapy. *Expert Rev. Anticancer Ther.* **7** (6), 833–837 (2007).
32. Nikolova, M. P. & Chavali, M. S. Metal oxide nanoparticles as Biomedical materials. *Biomimetics* **5** (2), 27. <https://doi.org/10.3390/biomimetics5020027> (2020).
33. Jain, K. K. Nanobiotechnology-based drug delivery to the Central Nervous System. *Neurodegenerative Dis.* **4**, 287–291. <https://doi.org/10.1159/000101884> (2007).
34. Erik, C. et al. The golden age: gold nanoparticles for biomedicine. *Chem. Soc. Rev.* **41**, 2740–2779. <https://doi.org/10.1039/C1CS15237H> (2012).
35. El-Deeb, N. M., El-Sherbiny, I. M., El-Aassar, M. R. & Hafez, E. E. Novel Trend in Colon cancer therapy using silver nanoparticles synthesized by Honey Bee. *Nanomed. Nanotechnol.* **6**, 265. <https://doi.org/10.4172/2157-7439.1000265> (2015).
36. Bromma, K. & Chithrani, D. B. Advances in gold nanoparticle-based Combined Cancer Therapy. *Nanomaterials* **10** (9), 1671. <https://doi.org/10.3390/nano10091671> (2020).
37. Khan, T. et al. Assessment of possible potential toxicity risks in albino mice exposed to amine coated silver nanoparticles, Kuwait Journal of Science 51 100172 (2024), (2024). <https://doi.org/10.1016/j.kjs.2023.100172>
38. Jeevanandam, J., Barhoum, A., Chan, Y. S., Dufresne, A. & Danquah, M. K. Review on nanoparticles and nanostructured materials: history, sources, toxicity, and regulations. *Beilstein J. Nanotechnol.* **9**, 1050–1074. <https://doi.org/10.3762/bjnano.9.98> (2018).
39. Hodayun, B., Lin, X. & Choi, H. J. *Challenges and Recent Progress in Oral Drug Delivery Systems for Biopharmaceuticals* 11129 (Pharmaceutics, 2019). 3 <https://doi.org/10.3390/pharmaceutics11030129>
40. Khalid, I. K., Khan, S. I. & Nanoparticles Properties, applications and toxicities. *Arab. J. Chem.* **12** (7), 908–931 (2017).
41. Sukhanova, A. et al. Dependence of Nanoparticle Toxicity on Their Physical and Chemical Properties, *Nanoscale Res Lett.* Feb 7:13(1):44 (2018). <https://doi.org/10.1186/s11671-018-2457-x>
42. Ortega, R., Devès, G. & Carmona, A. Biometal imaging and speciation in cells using proton and synchrotron radiation X-ray microscopy. *J. R Soc. Interface.* **6**, S649–S658 (2009).
43. Al-Qubaisi, M., Rozita, R., Yeap, S. K., Omar, A. R. & Ali, A. M. Alitheen, N. B. Selective cytotoxicity of goniothalamin against hepatoblastoma HepG2 cells. *Molecules* **16** (4), 2944–2959 (2011).
44. Borm, P., Robbins, D., Haubold, S. & Oberdorster, E. The potential risks of nanomaterials: a review carried out for ECETOC Part. *Part. Fibre Toxicol.* **3** (1), 11. <https://doi.org/10.1186/1743-8977-3-11> (2006).
45. Poh, T. Y. et al. Inhaled nanomaterials and the respiratory microbiome: clinical, immunological and toxicological perspectives. *Part. Fibre Toxicol.* **15** (46) (2018).
46. Li, J. J., Muralikrishnan, S., Ng, C. T., Yung, L. Y. L. & Bay, B. H. Nanoparticle-induced pulmonary toxicity. *Experimental Biology Med.* **235** (9). <https://doi.org/10.1258/ebm.2010.010021> (2010).
47. Sonvico et al. Surface-modified nanocarriers for nose-to-brain delivery. *Pharmaceutics* **10** (1), 34. <https://doi.org/10.3390/pharmaceutics10010034> (2018).
48. Saeed, M., Roya, H., Samani, J. & Aghaeivanda, S. Toxic effects of Silver nanoparticles on Liver and some hematological parameters in male and female mice (*Mus musculus*). *Biol. Trace Elem. Res.* **165** (2). <https://doi.org/10.1007/s12011-015-0247-1> (2015).
49. Nosrati, H. et al. The potential renal toxicity of silver nanoparticles after repeated oral exposure and its underlying mechanisms. *BMC Nephrol.* **22**, 228. <https://doi.org/10.1186/s12882-021-02428-5> (2021).
50. Rana, K., Verma, Y. & Rana, R. S. Renal toxicity of nanoparticles of cadmium sulphide in rat. *Chemosphere* **193**, 142–150. <https://doi.org/10.1016/j.chemosphere.11.011> (2018).
51. Duana, J., Yua, Y., Lib, Y., Yua, Y. & Sunab, Z. Cardiovascular toxicity evaluation of silica nanoparticles in endothelial cells and zebrafish model. *Biomaterials* **34** (23), 5853–5862. <https://doi.org/10.1016/j.biomaterials.2013.04.032> (2013).
52. Sharma, H. S., Ali, S. F., Hussain, S. M., Schlager, J. J. & Sharma, A. Influence of engineered nanoparticles from metals on the blood–brain barrier permeability, cerebral blood flow, brain edema and neurotoxicity. An experimental study in the rat and mice using biochemical and morphological approaches. *J. Nanosci. Nanotechnol.* **9** (8), 5055–5072 (2009).
53. Ansari, S. M. et al. C. V. Cobalt nanoparticles for biomedical applications: facile synthesis, physiochemical characterization, cytotoxicity behavior and biocompatibility. *Appl. Surf. Sci.* **414**, 171–187 (2017).
54. Li, S., Li, H., Xu, X., Saw, P. E. & Zhang, L. Nanocarrier-mediated antioxidant delivery for liver diseases. *Theranostics* **10** (3), 1262–1280 (2020). <https://www.thno.org/v10p1262.htm>
55. Abbasalipourkabira, R. et al. Toxicity of zinc oxide nanoparticles on adult male Wistar rats. *Food Chem. Toxicol.* **84**, 154–160 (2015).
56. Hosseini, S. M. et al. Chronic zinc oxide nanoparticles exposure produces hepatic and pancreatic impairment in female rats. *Iran. J. Toxicol.* **14** (3), 145–154. <https://doi.org/10.32598/ijt.14.3.626.1> (2020).
57. Abdallah, E. A. A study of sub-chronic genotoxic effects of zinc oxide nanoparticles and protective role vitamin E on stomach and pancreas in adult albino rats. *Egypt. J. Forensic Sci. Appl. Toxicol. Volume.* **18**, 25–41. <https://doi.org/10.21608/EJFSAT.2018.4194.1017> (2018).
58. García, A. I., de Blas, A. J. C. & Carabaño, R. Comparison of different methods for nitrogen and amino acid evaluation in rabbit diets. *Anim. Sci.* **80** (2), 169–178 (2005).
59. Kim, D., Jeong, S. & Moon, J. Synthesis of silver nanoparticles using the polyol process and the influence of precursor injection. *Nanotechnology* **17**, 4019–4024 (2006).
60. Arora, S., Sharma, P. & Kumar, S. Gold-nanoparticle induced enhancement in growth and seed yield of Brassica juncea. *Plant. Growth Regul.* **66**, 303–310. <https://doi.org/10.1007/s10725-011-9649-z> (2012).
61. Amiri, S. & Shokrollahi, H. The role of cobalt ferrite magnetic nanoparticles in medical science. *Mater. Sci. Eng.* **33**, 1–8. <https://doi.org/10.1016/j.msec.2012.09.003> (2013).
62. Ahmed, M. A., El-dek, S. I., Mansour, S. F. & Okasha, N. Modification of Mn nano-ferrite physical properties by gamma, neutron, and laser irradiations. *Solid StateSci.* **13**, 1180–1186 (2011).
63. Mansour, S. F., Hemeda, O. M., El-Dek, S. I. & Salem, B. I. *Magn. Mater. Magn. J.* **420**: 7–18 (2016).

64. Reitman, S. & Frankel, S. A colorimetric method for the determination of serum glutamic oxalacetic and glutamic pyruvic transaminases. *Am. J. Clin. Pathol.* **28** (1), 56–63 (1957).
65. Bancroft, J. D. & Gamble, M. *Theory and Practice of Histological Techniques* 6th edn pp. 725 (Churchill Livingstone/Elsevier, 2008).
66. Dippong, T., Levei, E. A. & Cadar, O. Investigation of Structural, morphological and magnetic properties of MFe_2O_4 ($M = Co, Ni, Zn, Cu, Mn$) obtained by Thermal decomposition. *Int. J. Mol. Sci.* **23**, 8483. <https://doi.org/10.3390/ijms23158483> (2022).
67. Singh, R. P. P., Hudia, I., Panday, S. & Rana, S. B. Effect of Ni doping on structural, optical, and magnetic properties of Fe-doped ZnO nanoparticles. *J. Supercond Nov Magn.* **28**, 3685–3691 (2015).
68. Ahamed, M. et al. S Iron oxide nanoparticle-induced oxidative stress and genotoxicity in human skin epithelial and lung epithelial cell lines. *Curr. Pharm. Des.* **19** (37), 6681–6690 (2013).
69. Horev-Azaria, L. et al. Predictive toxicology of cobalt ferrite nanoparticles: comparative in vitro study of different cellular models using methods of knowledge discovery from data. *Part. Fibre Toxicol.* **10**, 32 (2013).
70. Saquib, Q. et al. Zinc ferrite nanoparticles activate IL-1b, NFkB1, CCL21 and NOS2 signaling to induce mitochondrial dependent intrinsic apoptotic pathway in WISH cells. *Toxicol. Appl. Pharmacol.* **273** (2), 289–297 (2013).
71. Murdock, R. C., Braydich-Stolle, L., Schrand, A. M., Schlager, J. J. & Hussain, S. M. Characterization of nanomaterial dispersion in solution prior to in vitro exposure using dynamic light scattering technique. *Toxicol. Sci.* **101**, 239–253 (2008).
72. Nel, A., Xia, T., Madler, L. & Li, N. Toxic potential of materials at the nanolevel. *Science* **311**, 622–627 (2006).
73. Yu, K. O. et al. Toxicity of amorphous silica nanoparticles in mouse keratinocytes. *J. Nanopart. Res.* **11**, 15–24 (2009).
74. Nikam, D., Jadhav, S., Khot, V., Phadatare, M. & Pawar, S. Study of AC magnetic heating characteristics of $Co_{0.5}Zn_{0.5}Fe_2O_4$ nanoparticles for magnetic hyperthermia therapy. *J. Magn. Magn. Mater.* **349**, 208–213. <https://doi.org/10.1016/j.jmmm.2013.08.039> (2014).
75. Yaseneva, P., Bowker, M. & Graham, H. Structural and magnetic properties of Zn-substituted cobalt ferrites prepared by co-precipitation method. *Phys. Chem. Chem. Phys.* **13**, 18609–18614 (2011).
76. Hassadee, A., Jutarosaga, T. & Onreabroy Effect of zinc substitution on structural and magnetic properties of cobalt ferrite. *Procedia Eng.* **32**, 597–602 (2012).
77. Balakrishnan, P., Bala, S. & Niccolò, F. C. Tamara Exploiting Unique Alignment of Cobalt Ferrite Nanoparticles, mild hyperthermia, and controlled intrinsic cobalt toxicity for Cancer Therapy. *Adv. Mater.* **32**, 1–11. <https://doi.org/10.1002/adma.202003712> (2020).
78. Novotna, B. et al. The impact of silica encapsulated cobalt zinc ferrite nanoparticles on DNA, lipids and proteins of rat bone marrow mesenchymal stem cells. *Nanotoxicology* **10**, 662–670. <https://doi.org/10.3109/17435390.2015.1107144> (2016).
79. Noori, A., Karimi, F., Fatahian, S. & Yazdani, F. Effects of zinc oxide nanoparticles on renal function in mice. *Int. J. Biosci.* **5** (9), 140–146 (2014).
80. Nankivell, J. B. Creatinine clearance and the assessment of renal function. *Australian Prescriber.* **24** (1), 15–17 (2001).
81. Almansour, I. M., Alferah, A. M., Shraideh, A. Z. & Jarrar, M. B. Zinc oxide nanoparticles hepatotoxicity: histological and histochemical study. *Environ. Toxicol. Pharmacol.* **51**, 124–130 (2017).
82. Abdel-Aziz, O. H., Ragab, E. E. & Hamdan, M. H. The histological effects of zinc oxide nanoparticles on the kidney of adult male rabbits. *Sohag Med. J. Vol.* **22 No** (2), 297–301 (2018).

Acknowledgements

The authors would like to thank Prof. Dr. Osama Hemeda, Department of Physics, Faculty of Science, Tanta University who provided the assistance in the VSM discussion.

Author contributions

Sabry A. El-Naggar: Designed, conceived the study proposal, final revision of the manuscript, group coordinator and supervision. B. I. Salem: Carried out nanoparticle's preparation, participated in the study design, analyzing the data and wrote the paper. Eman E. El-Nahass, Mona M. Elwan: Equally conducted the experiment, Animal handling and dissecting, analyzed the data and wrote the paper. All authors contributed to the article and approved the submitted manuscript version.

Funding

Open access funding provided by The Science, Technology & Innovation Funding Authority (STDF) in cooperation with The Egyptian Knowledge Bank (EKB). The author(s) received no financial support for the research.

Declarations

Competing interests

The authors declare no competing interests.

Ethics approval

The animals were humanely treated, and the experimental design was approved by the Animal care committee at the Zoology Department, Faculty of Science, Tanta University (Protocol No.: IAUCUC-SCI-TU-0232) prior to performing the experiments.

Additional information

Correspondence and requests for materials should be addressed to B.I.S.

Reprints and permissions information is available at www.nature.com/reprints.

Publisher's note Springer Nature remains neutral with regard to jurisdictional claims in published maps and institutional affiliations.

Open Access This article is licensed under a Creative Commons Attribution 4.0 International License, which permits use, sharing, adaptation, distribution and reproduction in any medium or format, as long as you give appropriate credit to the original author(s) and the source, provide a link to the Creative Commons licence, and indicate if changes were made. The images or other third party material in this article are included in the article's Creative Commons licence, unless indicated otherwise in a credit line to the material. If material is not included in the article's Creative Commons licence and your intended use is not permitted by statutory regulation or exceeds the permitted use, you will need to obtain permission directly from the copyright holder. To view a copy of this licence, visit <http://creativecommons.org/licenses/by/4.0/>.

© The Author(s) 2025